

NUMERICAL INVESTIGATION OF INLET BOUNDARY CONDITION EFFECTS ON SECONDARY FLOWS IN LOW PRESSURE TURBINES

Seyfullah Cay* and Ayse G. Gungor†

Faculty of Aeronautics and Astronautics, Istanbul Technical University, Istanbul, Turkey

ABSTRACT

In this study, effects of incoming boundary layer (BL) profile on secondary flow structures are investigated by using an untwisted T106 turbine blade with large eddy simulation approach. Four different inlet boundary conditions are studied; a uniform inlet, a laminar BL profile inlet, turbulent BL profile inlet, and unsteady wake inlet with secondary flow structures. The computational effort is carried out using open source computational fluid dynamic solver OpenFOAM. Results indicate that the unsteady wake inlet boundary condition increases the turbulent kinetic energy activity and pressure losses significantly.

INTRODUCTION

Nowadays, the efficient use of energy is more significant than production of energy. Therefore, reducing the fuel consumption and emissions of the released harmful gases of aircraft engines has a great importance in terms of economically and environmentally in aviation. Reducing the weight of aircraft and increasing the efficiency of parts that significantly affect the performance of aircraft, such as wing and engine are some of the important solutions.

Gas turbine engines having huge weight are the most costly parts of an aircraft. Therefore, increasing the engine efficiency enables to reducing of fuel consumption, harmful gasses emissions, and size reduction.

Low pressure turbines (LPT) have a dominant role for whole engine efficiency because of the fact that power is produced by turbine. Although there are several ways to improve LPT efficiency, reducing the aerodynamic losses is one of the most important ways. Profile losses, due to the trailing edge thickness, and secondary flows are some of the most significant aerodynamic losses. Almost 30 – 50% of aerodynamic losses are due to the secondary flows [Sharma and Butler, 1987]. As a result of that, this research focuses on secondary flows. There are several secondary flow structures, however, suction side and pressure side leg of horseshoe vortices, and passage vortex are the most important secondary flow structures [Stephens, 2009]. These structures have substantial impact on the physics of an LPT flow, such as delaying (or eliminating) flow separation, enhancing heat transfer rates across the passage and so on [Goldstein and Spores, 1988].

*MSc. Student in Aero. and Astro. Eng., Email: cays@itu.edu.tr

†Assist. Prof. in Faculty of Aeronautics and Astronautics, Email: ayse.gungor@itu.edu.tr

Investigation of an LPT flow by means of experiments are costly and they require extremely large experimental setups. Direct numerical simulation (DNS), as far as computational methods are concerned, gives the most detailed information for the subject yet the computational time and cost requirements are still too high to afford [Gungor et al., 2012], [Karaca and Gungor, 2016]. Because of the flow field in LPT is always three-dimensional, viscous, highly unsteady, transitional, and turbulent, Reynolds averaged Navier-Stokes (RANS) is not capable of providing sufficient detail of the flow field compared to large eddy simulation (LES). LES gives sufficient physical insight to improve the understanding of turbulence by capturing large scale dynamics and modeling small scale structures and is feasible for such complex flow problems in terms of resolution, computational cost, and computational time.

In a previous study [Cay et al., 2016], we investigated the development of secondary flow structures and their influence on the suction side separation bubble by using the open-source computational fluid dynamics software OpenFOAM. Results show the predictive capability of OpenFOAM for LES LPT analysis using the k-equation subgrid model [Menon et al., 1996]. We also studied the effect of inflow turbulence on secondary flow structures. In that study, a uniform inlet profile with different levels of turbulence intensity is introduced at the inflow. Results on a relatively coarse LES mesh showed that the inlet characteristics play a significant role on the development of secondary flow structures.

The purpose of this study is to investigate the effect of realistic inlet conditions on secondary flow structures and losses on a *T106* blade.

The paper begins with a brief discussion of the numerical methodology and description of steady and unsteady inlet boundary conditions. This is followed by a discussion of the results, beginning with the validation of the LES solver for turbine flows without endwall, followed by a grid resolution effect and overall features of the flow field with endwall simulations. Then effects of steady and unsteady inlet boundary conditions on secondary flows and losses are examined. The paper concludes with a summary of the main results.

NUMERICAL DETAILS

The simulations are performed by using open source computational fluid dynamics software OpenFOAM. The solver solves the three-dimensional, unsteady LES equations with a finite volume method. The untwisted *T106* turbine blade profile on linear cascade is used in this study. The pressure implicit splitting of operators algorithm (PISO) is employed with second order schemes in order to account for the unsteady turbulence. A constant time step for which the Courant stability is less than one is used. One eddy equation subgrid model, which is also known as k-equation model, is used for this study since we saw in a previous study [Cay et al., 2016] that Smagorinsky model [Smagorinsky, 1963] gives more dissipative results than the k-equation subgrid model.

The specifications of the *T106* turbine blade are given in table 1. Computational domain and boundary conditions are shown in figure 1. No slip boundary condition is applied to blade surface and endwall. Periodic boundary condition is applied on blade side surfaces in order to include effects of adjacent

Chord, c	198	[mm]
Axial chord, C_{ax}	170	[mm]
Blade stagger	30.7	[°]
Pitch	158	[mm]
Span, s	375	[mm]
Inlet flow angle	37.7	[°]
Design exit flow angle	63.2	[°]

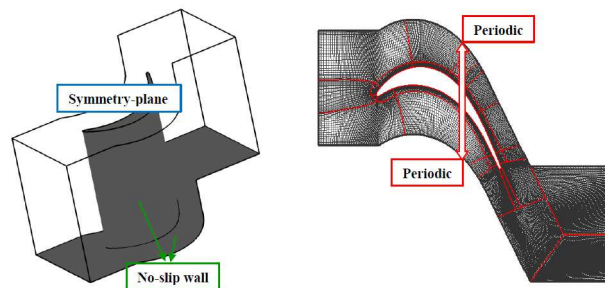


Table 1: *T106* blade specifications. Figure 1: Geometry, boundary conditions, and mesh structure

blades on the flow field. Half span is used for all simulations with symmetry plane boundary condition. Reynolds number based on the reference inlet velocity, chord length and kinematic viscosity is 8×10^4 .

Inlet Boundary Conditions

To investigate the effect of steady and unsteady inlet boundary conditions on secondary flows and losses four different simulations with endwall are performed. Three of these simulations have steady inlet boundary condition. First one has a uniform inlet, second one has a laminar boundary layer (LBL) profile inlet with a shape factor of 2.2, and the third one has a turbulent boundary layer (TBL) profile inlet with a shape factor of 1.5. LBL and TBL inlet velocity profiles are taken from [Cui et al., 2016]. Only the mean velocity profiles are imposed in the TBL inlet simulation.

The last simulation is carried out to investigate the unsteady stator-rotor interaction. In order to mimic this interaction, the inlet velocity profile is taken from the wake region (approximately $0.18 C_{ax}$ from trailing edge) of the simulation with TBL inlet condition. It is flipped and introduced as time varying inflow condition with approximately 0.6 Strouhal number ($St = \frac{c f}{U_{in}}$). Here, c is the chord length, f is the wake passing frequency, and U_{in} is the inlet velocity. Figure 2 shows the set-up of this boundary condition and inlet velocity profiles at several wake passing periods.

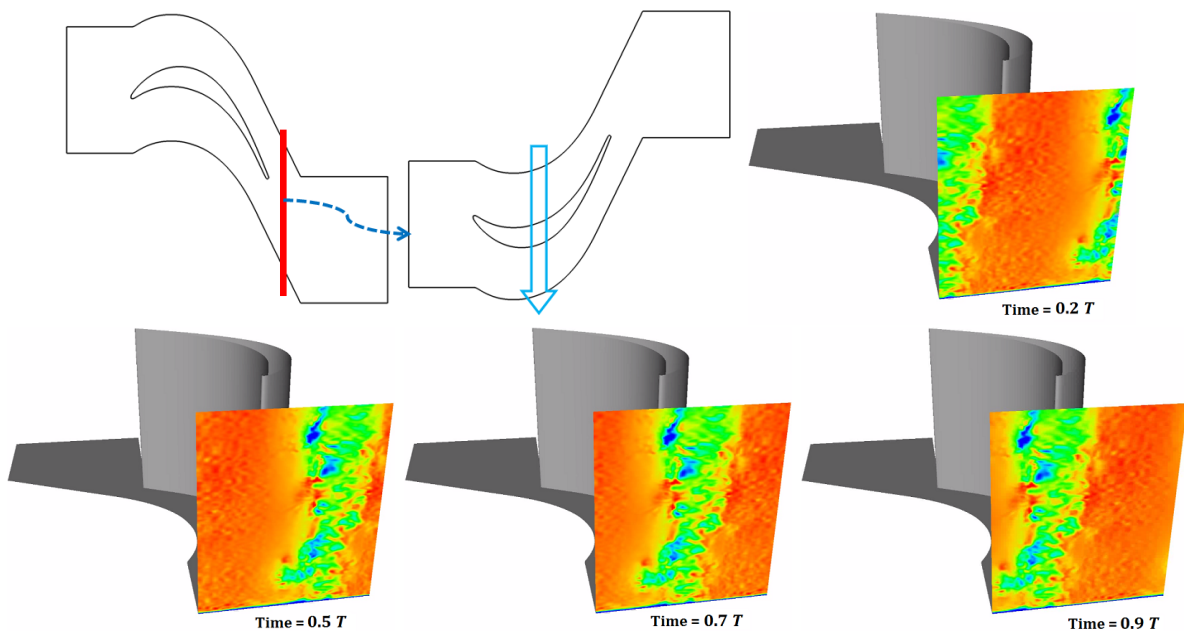


Figure 2: Unsteady wake inlet profile.

For all simulations turbulent statistics are accumulated for ten flow through times (FTT) after an initial transient of five FTT.

RESULTS

Code Validation

In order to show the capabilities of the LES solver, we first performed an analysis without endwall along the $T106$ blade. This simulation has a uniform inflow condition and approximately 3 million structured grid points. Also it has 45° inflow angle for validation. We compared our LES results with an experimental and incompressible DNS data of [Wissink, 2006] and compressible DNS data of [Sandberg et al., 2012] as shown in Fig. 3.

The mean pressure distribution along the suction and pressure sides of the blade shows excellent agreement with the experimental data, and fairly good agreement with DNS data.

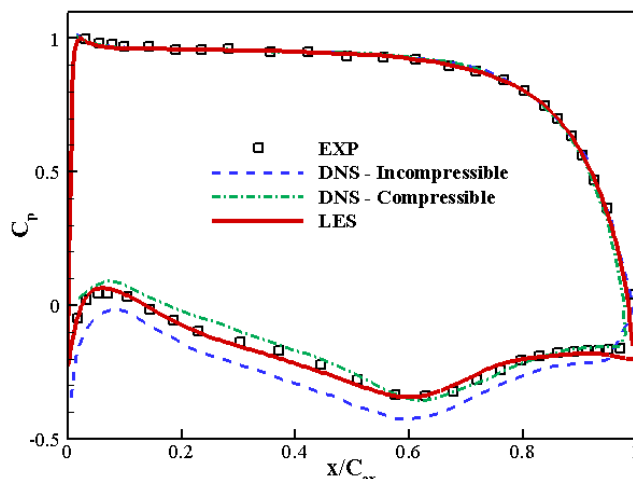


Figure 3: Mean pressure coefficient. Simulation is performed without endwall.

Grid Resolution Effect

The sensitivity of the results to the grid resolution is investigated in this section. We performed three different simulations; coarse grid with 3 million grid points, medium grid with 15 million points, and fine grid with 30 million points to identify the most appropriate grid for the LES of T106 turbine blade with an endwall. For these studies the TBL inlet profile boundary condition is used.

The coarse grid provided the accuracy of the simulation inputs by the validation of pressure coefficient distribution and also the determination of a suitable LES model. However, coarse grid simulation does not have sufficiently small grid size to resolve the relevant scales of the flow, while two other grids are found to be fine enough for an LES study. Therefore, fine and medium grids have taken into account for the investigation of secondary flow structures.

The proficiency in fine and medium grid resolutions are examined by studying the spectra of the resolved turbulent kinetic energy (TKE) at a probe located in wake region at $0.5 C_{ax}$ from the trailing edge and $0.1 z/s$ from the endwall. Although this location is a bit far away from the endwall and blade surface, both grids provide Kolmogorov's $-5/3$ law for at least one order as shown in Fig. 4 (a). The energy level of large eddies in the simulation with 15 million grid points is greater than fine case with 30 million grid points. As the resolution increases more and more fine structures are resolved.

Figures 4 (b) and (c) show the instantaneous second invariant of velocity gradient tensor [Hunt et al.,

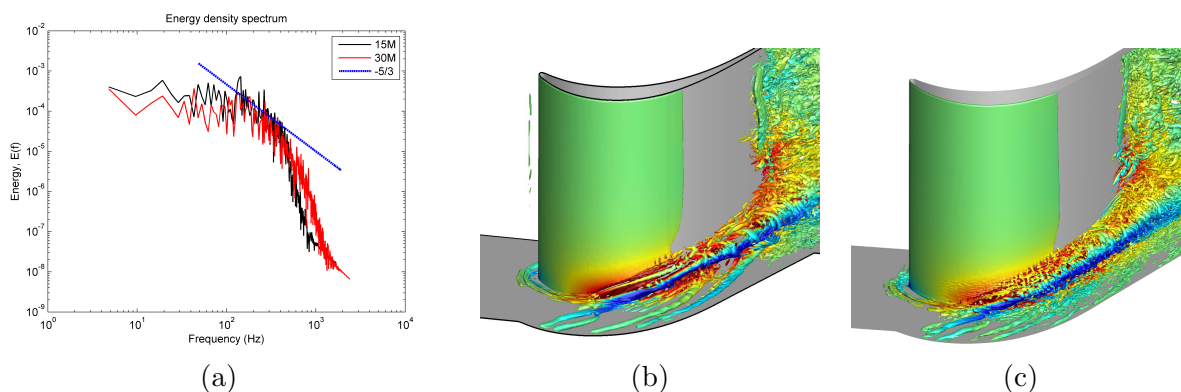


Figure 4: (a) Energy density spectrum for simulations with 15 and 30 million grid points. Instantaneous second invariant of the velocity gradient tensor colored by spanwise velocity, (b) 15 million grid points, (c) 30 million grid points.

1988] coloured by the spanwise velocity for fine and medium grid simulations. As seen from the figure, fine grid case shows more intense, small-scale vortical structures near the end-wall and downstream of the separation bubble. However, the case having 15 million grid points is also fine enough to capture the relevant secondary flow structures: passage vortex, horseshoe vortices, corner vortices, counter vortex, and crossflows structures. Hence this grid is chosen for rest of the simulations presented in this study.

Overall Features of the Flow Field with Endwall

The general features of the endwall vortical structures from mean flow field for the TBL inlet case are visualised using the second invariant of velocity gradient tensor and shown in figure 5 (a). One of the most predominant vortical structure is the horseshoe vortex. When the incoming flow field with boundary layer encounters with LPT blade, saddle point occurs as shown in figure 5 (b) before arriving at the leading edge. The flow field is divided into two legs that start to rotate after the saddle point. These rotating flows, also known as horseshoe vortices, are amongst the most important reasons for the formation of losses and other secondary flow structures. The pressure side leg of the horseshoe vortex separates at the saddle point, rolls toward the suction side surface of neighboring blade. Then it becomes the passage vortex. Corner vortices are also observed near the intersection of the suction side of the blade and endwall. The crossflow as a result of the transverse pressure gradient from the neighbouring blade rolls around the corner vortices as shown in figures 5 (a) and (b).

Figure 5 (c) shows the streamlines of the mean flow field on the suction side surface of the blade for the TBL inflow case. Separation line shows the boundary between the laminar flow and the separated flow over the blade suction side. It is apparent that there is no separation near the endwall due to the presence of passage vortex. The traces of passage vortex and corner vortex on the blade surface are also apparent in figure 5(c).

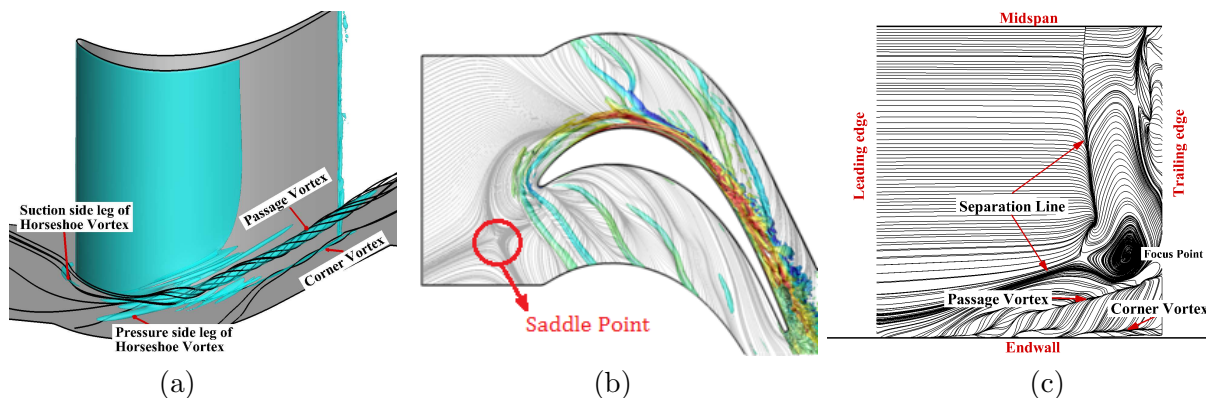


Figure 5: (a) Second invariant of the velocity gradient tensor iso-surfaces and streamlines computed from the mean flow field for TBL inlet case, (b) Streamlines of the mean flow field on the endwall along with the instantaneous second invariant of the velocity gradient tensor isosurfaces colored by spanwise velocity, (c) Streamlines of the mean flow field on the blade suction surface.

Figure 6 presents the mean pressure coefficient for the LES studies with TBL inlet condition in comparison to experimental and DNS data [Koschichow et al., 2014]. DNS and experimental data were taken at midspan region. Distribution of LES pressure coefficient along the blade surface is presented at five spanwise slices. Locations of these slices in spanwise direction range from near endwall to midspan.

It is apparent from figure 6 that there are differences in pressure coefficient between near endwall and midspan on the leading edge side of the suction surface due to the horseshoe vortex. Horseshoe vortex and leading edge corner vortex cause pressure loss on the leading edge side. The yellow line in figure 6 shows nearly starting point of passage vortex. So passage vortex starts approximately $x/C_x \approx 0.3$ near the endwall region. The effects of passage vortex, counter vortex, corner vortex, and cross flows on pressure distribution are apparent at $z/s = 1\%$ and $z/s = 2.5\%$ near endwall region.

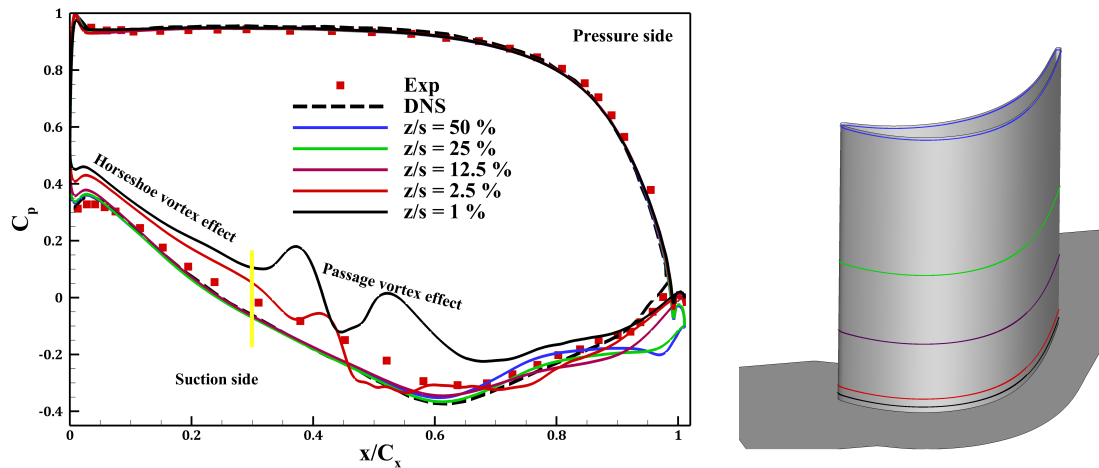


Figure 6: Mean pressure coefficient and locations of slices in spanwise direction.

Effect of Inflow Condition

Figures 7 (a-d) illustrate contour plots of turbulent kinetic energy (TKE) in y - z planes according to four different inlet conditions at axial locations of $x/C_x = 0.50, 0.75, 1.00,$ and 1.30 . The passage vortex and boundary layer separation on the suction side of the blade are the main source of turbulent fluctuations. At the downstream of the trailing edge, the vortical structures become complicated due to interaction between passage vortex, separation vortices, and wake vortices. As shown in the figure, most of the endwall region and blade suction surface involve high turbulent fluctuations. High levels of TKE in passage vortex are consistently observed throughout the blade passage for all simulations.

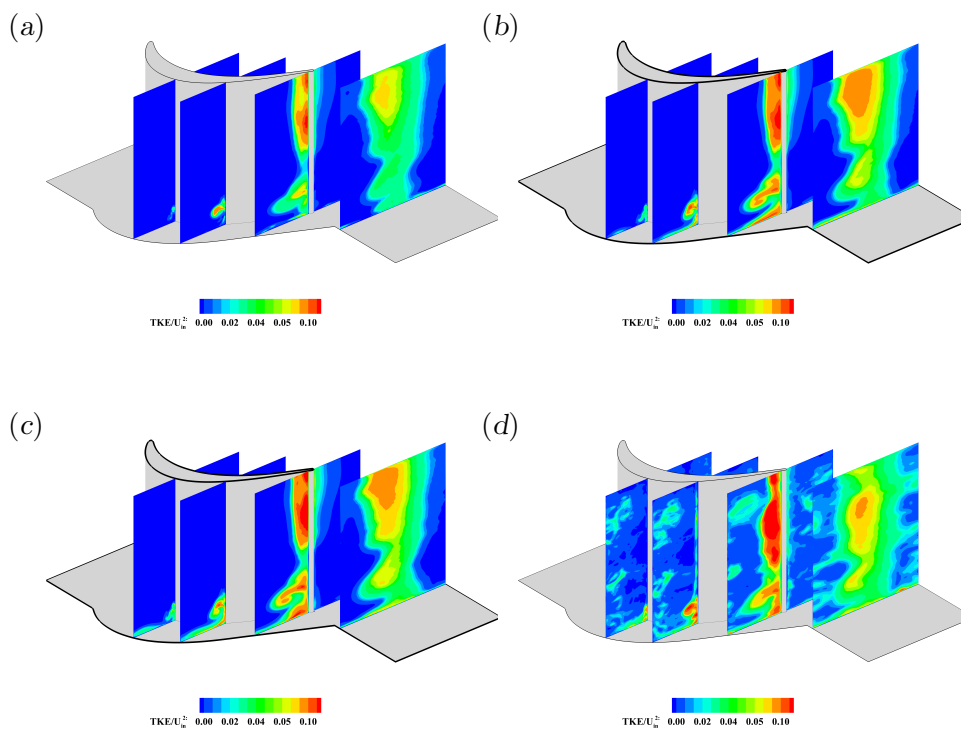


Figure 7: Contour plots of mean turbulent kinetic energy in y - z planes at $x/C_x = 0.50, 0.75, 1.00,$ and 1.30 . (a) Uniform inlet, (b) LBL inlet, (c) TBL inlet, (d) Unsteady wake inlet with secondary flow.

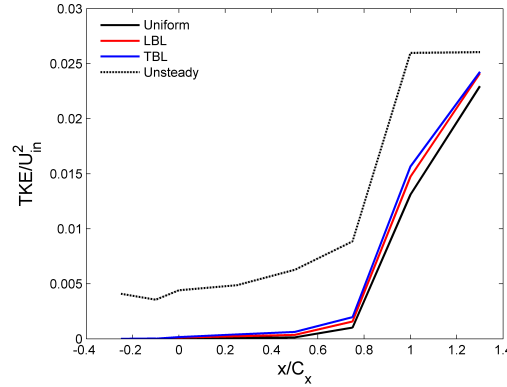


Figure 8: Area weighted average of mean TKE distribution along the streamwise direction.

For the TBL and unsteady wake cases, there is also strong turbulence activity near the endwall due to the crossflow structures from the neighbouring blade. Secondary flows in uniform inlet has smaller structures and lesser TKE in comparison with other inlet conditions. However, this inlet condition is far from realistic turbine inlet condition. The passage vortex in unsteady inlet condition has stronger TKE (see at axial location of $x/C_x = 0.75$) due to wake passing. The secondary flows with higher TKE cause more pressure loss. As a result, secondary losses of the simulation with unsteady realistic inlet condition are higher than other inlet conditions.

Figure 8 shows the area weighed average of mean TKE distribution along the streamwise direction for four different inlet conditions. In all steady simulations, the turbulence levels are approximately zero at the leading edge of the blade. While for the unsteady case, there is significant turbulent activity due to the wake passing. For all cases, TKE level increases significantly after $x/C_x = 0.75$ as a result of the separated region and secondary flows near endwall. TKE levels are higher in the simulation with the unsteady wake inlet in comparison with the other inlet boundary conditions. Leading to the fact that more energy is transferred from the mean flow to the turbulent structures. Hence, it can be said that the pressure and energy losses are more with the unsteady wake inlet. These results indicate that inlet condition appears to be quite important for secondary flows and losses.

In order to investigate the unsteady feature of the wake simulation, the temporal variation of the spanwise velocity along one wake-passing period is studied. Figure 9 (a-c) and (e-g) show spanwise velocity distribution for $z/s = 1\%$ and 2.5% planes, respectively. $z/s = 1\%$ plane is a significant plane to investigate the effects of unsteady wake inlet boundary condition on the horseshoe vortex, starting point of the passage vortex on the suction side, corner vortices, and crossflows during a wake passing period. Figure indicates that these structures are strongly influenced by the wake-passing. The strength and location of the endwall structures constantly vary with time, contrary to Uniform, LBL, and TBL inlet conditions. This situation increases the unsteady activity and creates more complex flow field. Thus, even if the realistic inlet condition reduces and shrinks the separation area on the blade, the total loss increases because of the secondary flows. Furthermore, $z/s = 2.5\%$ plane indicates that the size of the passage vortex is highly variable during a wake passing period. These observations can be also seen from figures 9 (d) and (h) that show the spanwise velocity distribution along one wake passing period for $z/s = 1\%$ and $z/s = 2.5\%$ slices of the suction surface, respectively. The starting point and the strength of the passage vortex varies during the wake passing. In conclusion, these results clearly indicate that it is necessary to examine the velocity distributions in such planes for an effective design to reduce the secondary losses.

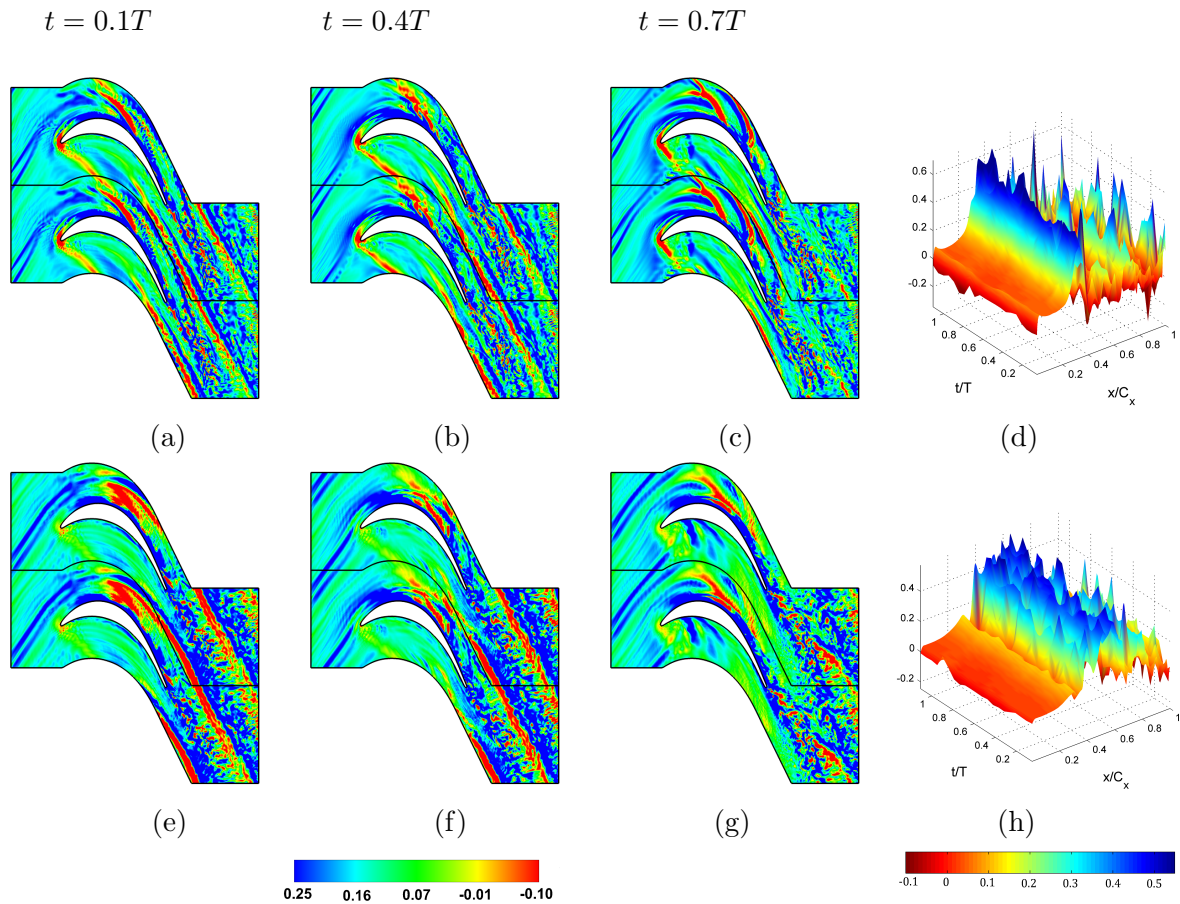


Figure 9: Spanwise velocity distribution at (a-c) $z/s = 1\%$ and (e-g) $z/s = 2.5\%$ planes for unsteady wake inlet with secondary flows along 1 wake passing. (d) and (h) are spanwise velocity distribution along one wake passing for $z/s = 1\%$ and $z/s = 2.5\%$ slices of the suction surface.

CONCLUSION

In this work effects of inflow boundary conditions on secondary flows are studied by means of LES using OpenFOAM. Results indicate that the application of realistic unsteady wake inlet boundary condition significantly increases the TKE activity and pressure losses. Besides, the strength of passage vortex increases due to increasing cross flow motions. Results demonstrate the need to consider realistic inflow conditions in turbine blade analysis and design.

ACKNOWLEDGEMENTS

This work is partly funded by 2016 Research Specialist Training program (ITU-AYP) under grant number ITU-AYP-2016-15.

References

- Cay, S., Karahan, D.T. and Gungor A.G. (2016) *Large Eddy Simulation of Endwall Flows in Low Pressure Turbines*, Ninth International Conference on Computational Fluid Dynamics, Turkey, July 2016,
- Cui, J., Nagabhushana Rao, V., and Tucker, P. G., (2016) *Numerical investigation of secondary flows in a high-lift low pressure turbine*, International Journal of Heat and Fluid Flow, 2016,

- Goldstein, R. and Spores, R. (1988) *Turbulent transport on the endwall in the region between adjacent turbine blades*, Journal of Heat Transfer, Vol 110, p: 862-869, NOVEMBER 1988,
- Gungor, A. G., and Simens, M. P., and Jiménez, J. (2012) *Direct numerical simulations of wake-perturbed separated boundary layers*, Journal of Turbomachinery, Vol 134, p: 061024, 2012,
- Hunt, J. C. R., and Wray, A. A., and Moin, P., (1988) *Eddies, stream, and convergence zones in turbulent flows*, Center for Turbulence Research Report, p: 193-208, 1988,
- Karaca, S., and Gungor, A.G. (2016) *DNS of unsteady effects on the control of laminar separated boundary layers*, European Journal of Mechanics B/Fluids, Vol 56, p: 71-81, 2016,
- Koschichow, D., Fröhlich, J., Kirik, I., and Niehuis, R., (2014) *Dns of the flow near the endwall in a linear low pressure turbine cascade with periodically passing wakes*, ASME paper GT2014-25071, 2014,
- Menon, S., Yeung, P.K., and Kim., W.W., (1996) *High Reynolds number flow simulations using the localized dynamic subgrid-scale model.*, AIAA Paper 1996-0425,
- Sandberg, R.D., Pichler, R. and Chen, L. (2012) *Assessing the sensitivity of turbine cascade flow to inflow disturbances using direct numerical simulation*, 13th International Symposium for Unsteady Aerodynamics, Aeroacoustics and Aeroelasticity in Turbomachinery (ISUAAAT), Tokyo, 2012,
- Sharma, O.P. and Butler, T.L. (1987) *Predictions of Endwall Losses and Secondary Flows in Axial Flow Turbine Cascades*, Journal of Turbomachinery, Vol 109, p: 229-236, April 1987
- Smagorinsky, J., (1963) *General circulation experiments with the primitive equations I The basic experiment.*, Monthly Weather Review, Vol 91, p: 99-164, 1963,
- Stephens, J. E. (2009) *Control of the tip-gap flow of a low pressure turbine blade in a linear cascade*, Ph.D. thesis, April 2009
- Wissink, J.G. and Rodi, W. (2006) *Direct Numerical Simulations of Transitional Flow in Turbomachinery*, Journal of Turbomachinery, Vol 128, p: 668-678, October 2006,